

Coiling of Viscous Liquids

Fábio Cruz (n.69476)¹

¹Departamento de Física, Instituto Superior Técnico, Universidade de Lisboa, Lisboa, Portugal

A thin “rope” of viscous fluid falling from high enough coils upon contact with a rigid surface. This coiling is controlled by the balance between the three main forces acting on the fluid: viscous, gravitational and inertial forces. We introduce the key aspects of the theoretical framework used to describe slender viscous jets, and compare the scaling laws governing the gravitational and inertial coiling regimes with experimental data. Despite limitations of the experimental setup, we find good agreement with theoretically predicted trends.

I. INTRODUCTION

A stream of viscous fluid falling from a sufficient height approaches a surface in the form of a rotating coil. The simplest example of such behaviour, usually called “liquid rope coiling”, can be observed when pouring a thin stream of honey onto a toast. This phenomenon is an example of a buckling instability, in which a fluid becomes unstable by bending due to an axial compressive stress. Other examples of buckling instabilities are the periodic folding/coiling of lava streams [1] and the jet filling of containers [2], with applications in geophysics and food processing, respectively.

Although fluid coiling has been studied for over 50 years [3][4], only recently the mechanisms that determine the behaviour of these systems have been explored with greater depth. In 2004, Ribe [5] proposed that the dynamics of a thin stream of viscous fluid are determined by the relative magnitudes of viscous, gravitational and inertial forces. Moreover, he demonstrated numerically the existence of three coiling regimes, depending on the fall height and flow rate.

In this work we present a compact introduction to the theoretical framework used to describe coiling liquid ropes¹ (section II) and compare the force-balance predictions for the coiling frequency with results obtained in a homemade experiment (sections III-IV).

II. THEORETICAL FRAMEWORK

Our objective in the following text is to illustrate the guidelines to derive the dependence of the coiling frequency Ω on the fluid’s fall height H and flux rate Q (see Fig. 1 a)). The flux is considered to be constant and injected from a circular hole of radius a_0 . The liquid is characterized by its density ρ and kinematic viscosity ν . The rotating liquid column consists of a long, almost vertical tail and a coil next to the surface, of radius R . During the fall, the jet’s radius decreases due to gravity stretching, such that at the coil its value is $a_1 < a_0$.

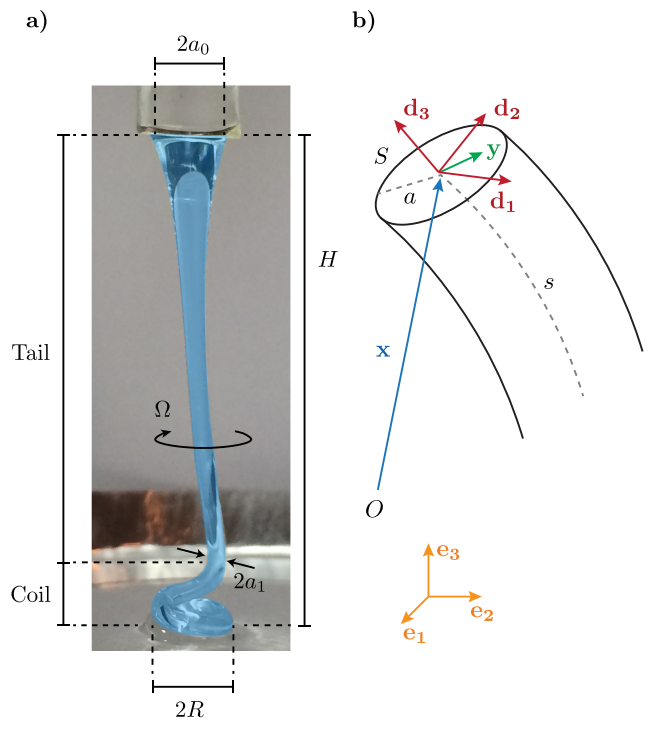


FIG. 1: a) Main parameters used to describe the coiling of viscous liquids; b) Geometry considered in the slender jet approximation (modified from [5]).

By exploiting the jet’s slenderness (i.e., the fact that the typical length scale for the variations of the flow variables is much larger than the jet’s radius), we can describe the dynamics of this system as those of a curved line. We choose this line to be the jet’s axis, parametrised by the coordinate $s \in [0, \ell]$, where $s = 0, \ell$ represent the points of injection and contact with the surface, respectively. For each point s , three orthogonal vectors \mathbf{d}_α are defined, where \mathbf{d}_3 is perpendicular to the circular jet’s cross section plane and $\mathbf{d}_{1,2}$ are arbitrary vectors in this plane (see Fig. 1 b)). Any fluid element lying on the jet’s cross section S is described by the coordinates $\mathbf{r} = \mathbf{x} + \mathbf{y}$ in the laboratory coordinate system \mathbf{e}_α , where \mathbf{x} is the jet’s axis position and $\mathbf{y} = y_1 \mathbf{d}_1 + y_2 \mathbf{d}_2$ is the position of the fluid element relative to it.

To derive the equations for the global force and torque

¹ The analysis performed here follows closely [5]. Refer to the full text for further details.

balances on the jet, we need to integrate the Navier-Stokes equation across the jet's cross section. The important dynamical quantities arising in this integration are the stress vector \mathbf{N} and the bending/twisting moment vector \mathbf{M} , defined by

$$\mathbf{N} \equiv N_\alpha \mathbf{d}_\alpha = \int_S \boldsymbol{\sigma} dS, \quad (1a)$$

$$\mathbf{M} \equiv M_\alpha \mathbf{d}_\alpha = \int_S \mathbf{y} \times \boldsymbol{\sigma} dS, \quad (1b)$$

where $\boldsymbol{\sigma}$ is the stress vector acting on the fluid elements, in which the viscous behaviour is embedded. The components N_α and M_α represent the fluid's resistance to stretching and bending/twisting, respectively.

The integrated force balance equation is

$$\rho A [\boldsymbol{\Omega} \times (\boldsymbol{\Omega} \times \mathbf{x}) + 2\boldsymbol{\Omega} \times \mathbf{U} + \mathbf{U}\mathbf{U}'] = \mathbf{N}' + \rho \mathbf{Ag}, \quad (2)$$

where $A = \pi a^2$ is the area of the jet's cross section, $\boldsymbol{\Omega} = \Omega \mathbf{e}_3$ is the coiling angular speed vector, $\mathbf{U} = U \mathbf{d}_3$ is the fluid axial velocity and $\mathbf{g} = -g \mathbf{e}_3$ is the gravitational acceleration. The three terms on the left-hand side of this equation represent the centrifugal and Coriolis forces and the axial acceleration, respectively. These inertial terms are balanced by the two terms on the right-hand side, which represent the jet's viscous resistance to deformation and gravitational effects. The derivatives present in this equation (and others that follow) are in respect to s .

The resultant torque balance equation is

$$0 = \mathbf{M}' + \mathbf{d}_3 \times \mathbf{N}, \quad (3)$$

where the angular acceleration and the gravity-induced torque were neglected by considering the jet is slender.

As stated before, it is the competition between viscous, gravitational and inertial forces at the coil that determines the dynamics of the jet. To estimate the different forces acting on the jet at this point (quantities with subscript 1), we need first to estimate the magnitude of the bending moment vector M . Standard dimensional analysis yields

$$M \sim \rho \nu \frac{a_1^4 U_1}{R^2}. \quad (4)$$

Combining this estimate with eqs. (2) and (3) and noting that $d/ds \sim R^{-1}$ in the coil, we find

$$F_{\text{viscous}} \sim \rho \nu a_1^4 U_1 R^{-4}, \quad (5a)$$

$$F_{\text{gravitational}} \sim \rho g a_1^2, \quad (5b)$$

$$F_{\text{inertial}} \sim \rho a_1^2 U_1^2 R^{-1}. \quad (5c)$$

Note that each force is directly proportional to the quantities that describe their driving mechanism, i.e. $F_{\text{viscous}} \propto \nu$, $F_{\text{gravitational}} \propto g$ and $F_{\text{inertial}} \propto U_1^2$.

Depending on how the viscous forces are balanced, three coiling modes are possible. The simplest case occurs for small fall heights. In this regime (viscous

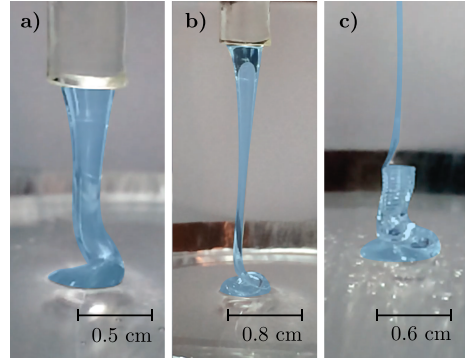


FIG. 2: Pictorial representation of the three coiling regimes: a) Viscous regime; b) Gravitational regime; c) Inertial regime. Note that picture c) was zoomed on the coil region to capture the small helical coiling structure.

regime), both gravity and inertia are negligible and the net viscous force on each fluid element is zero. The radius of the jet is nearly constant, $a_1 \approx a_0$, and the liquid behaves like toothpaste squeezed from a tube (see Fig. 2 a)). From dimensional analysis and the general relation $\Omega \sim U_1/R$, we find the scaling laws

$$R \sim H \equiv R_V, \quad (6a)$$

$$\Omega \sim a_1^{-2} Q H^{-1} \equiv \Omega_V. \quad (6b)$$

Increasing the fall height, we find the gravitational regime. In this regime, the jet's radius is no longer constant due to gravity-induced stretching (see Fig. 2 b)). The viscous forces acting on the fluid are balanced by gravity, such that we can derive the scaling laws

$$R \sim (\nu Q/g)^{1/4} \equiv R_G, \quad (7a)$$

$$\Omega \sim g^{1/4} \nu^{-1/4} a_1^{-2} Q^{3/4} \equiv \Omega_G. \quad (7b)$$

Further increasing the fall height triggers inertial effects (see Fig. 2 c)) due to the fact that the fluid velocity in the tail is much bigger than that at the injection point, $U_1/U_0 \gg 1$. In this case (inertial regime), viscous forces are balanced by inertia and the scaling laws are

$$R \sim \nu^{1/3} a_1^{4/3} Q^{-1/3} \equiv R_I, \quad (8a)$$

$$\Omega \sim \nu^{-1/3} a_1^{-10/3} Q^{4/3} \equiv \Omega_I. \quad (8b)$$

To complete the above scaling laws, we need to find a_1 . The jet's radius in the coil is controlled by the gravity-induced stretching that occurs in the tail. A simple model to describe the jet's radius along the fluid column is obtained by taking the \mathbf{d}_3 component of the force balance equation (2) and assuming unidirectional stretching (along the jet axis). The differential equation describing the fluid velocity component U is, in this case,

$$3\nu U (U'/U)' + g - UU' = 0. \quad (9)$$

The three terms in this equation represent the viscous resistance to stretching, gravity and inertia, respectively. The boundary conditions for this simple model



FIG. 3: Experimental setup: 1) plastic container with volumetric scale; 2) silicon oil ($\nu = 100 \text{ cm}^2/\text{s}$); 3) vertical holder; 4) ruler to be used as a reference spatial scale; 5) thin aluminium tray.

are $U(0) = U_0$ and $U'(H_1) = 0$, where $H_1 < H$ is the effective height at which the stretching vanishes. In the case of steady flux, the value of a_1 can then be obtained from the solution for U_1 by the relation $a_0^2 U_0 = a_1^2 U_1$.

A numerical solution for the above model with $U_0 = 0.54 \text{ cm/s}$ and $\nu = 100 \text{ cm}^2/\text{s}$ is shown in Fig. 5. For the parameters used, one finds the rough dependence $a_1 \propto H_1^{-1}$ in the range $1 < gH_1^2/\nu U_0 < 10^3$ of the effective gravity number. Assuming H_1 is a constant fraction of the total height H , we can express a_1 as a function of the external parameters H , Q , a_0 and ν and complete the scaling laws (7b) and (8b), hence obtaining

$$\Omega_G \propto H^2, \quad \Omega_I \propto H^{10/3}. \quad (10)$$

III. METHODS

In order to verify the scaling laws derived in the previous section, a simple homemade experiment was designed. The experimental apparatus consists of a plastic container (with a volumetric scale with intervals of 10 cm^3) and a holder that allows the control of the vertical position of the container (see Fig. 3). The liquid used was a silicon oil of viscosity $\nu = 100 \text{ cm}^2/\text{s}$ [6]. A thin aluminium tray was used to recycle the oil and a ruler was attached to a vertical bar to be used as a reference spatial scale.

The liquid was held in the plastic container by a screw on the bottom of radius $a_0 = 0.2 \text{ cm}$. When the screw was removed, the liquid started flowing down, hitting the aluminium tray and starting to coil. Because the flow was driven by the sum of atmospheric and fluid pressures, the rate Q was not constant and therefore the coiling was not steady. Although, considering a small time interval, the flow could be assumed approximately constant and the theory presented before applies. To check the validity

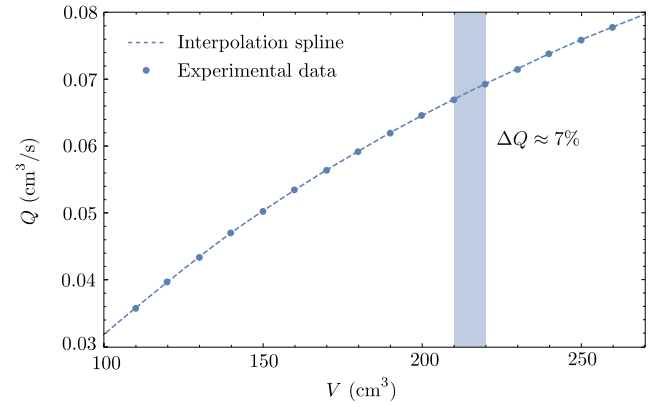


FIG. 4: Flux curve as a function of the volume of oil inside the container.

of this assumption, the volume of oil inside the container was measured as a function of time for a fixed fall height. The flux was then calculated by differentiating the interpolation curve for the volume as a function of time. The resultant flux curve is represented in Fig. 4 as a function of V , the volume of oil inside the container. As expected, the flux decreases as the fluid volume decreases. Nevertheless, in a volume interval of 10 cm^3 , the flux is nearly constant. For example, in the interval $220 - 210 \text{ cm}^3$ we observe a difference in the flux of about 7%. This volume interval corresponds to a period of approximately 5 minutes.

This volume interval was thus chosen to measure Ω and a_1 as a function of the fall height. Starting at $H = 3 \text{ cm}$ and with increments of 0.5 cm , the jet's motion was recorded with a 60 frames per second camera. The few initial seconds of motion (corresponding to the onset of coiling) were ignored and only the following $10 - 20$ seconds were considered as steady coiling. The flux was interrupted between measurements to reset the fall height. The values of a_1 and Ω were measured from the recorded movies with the video analysis software *Tracker* [7].

IV. RESULTS AND DISCUSSION

The experimental results obtained for the jet's radius a_1 were compared to the simple analytical model discussed in section II (see Fig. 5). The effective height H_1 was chosen to be a fraction of the total height, $H_1 = fH$. The value obtained for f was about 0.45. This value represents a shift on the horizontal axis and does not have an impact on the scaling $a_1 \propto H^{-1}$ observed.

Within the described set of parameters, the coiling frequency should thus follow the scaling laws (10). The experimental data for Ω is shown in Fig. 6, as well as the best fits for the two regions identified as corresponding to the gravitational and inertial regimes (consistently with the observations). The slopes of the dotted and dashed

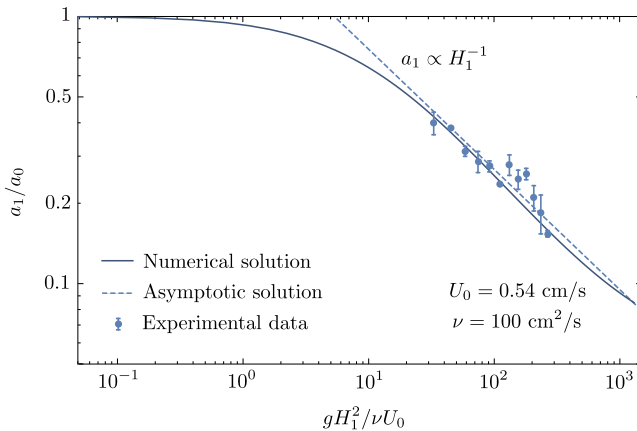


FIG. 5: Gravity-induced stretching of the jet radius: comparison between the numerical solution for the model presented in eq. (9) with $U_0 = 0.54$ cm/s and $\nu = 100$ cm²/s and the experimental results.

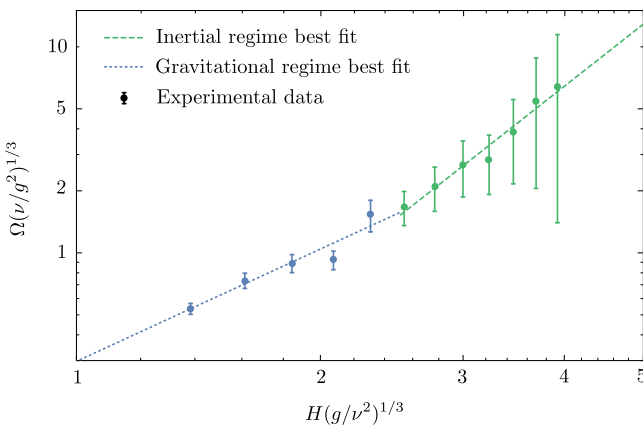


FIG. 6: Coiling frequency scaling laws: experimental data and best fits for the gravitational and inertial regimes.

lines are $\alpha_G = 1.81 \pm 0.33$ and $\alpha_I = 3.09 \pm 0.24$, respectively. These results are consistent with the values $\alpha_G^{\text{th}} = 2$ and $\alpha_I^{\text{th}} = 10/3$ predicted by the scaling laws (10). The two experimental points that lie before the transition between the gravitational and inertial regimes (see Fig. 6) show a more significant deviation from the

best fit for the first region presented. For these heights, the coiling of the jet was chaotic around the presented averages, which is a signature of a complex transition regime from the gravitational and inertial regimes whose analysis is out of the scope of this work.

The errors shown in Figs. 5 and 6 were estimated by the difference to the average of three independent measurements of a_1 and Ω . The increase in the magnitude of the error bars in Fig. 6 is due to the fact that for higher frequencies we approached the Nyquist sampling frequency of the camera used. The asymmetry on the error bars is a consequence of the logarithmic scale used to represent the data.

V. CONCLUSIONS

Despite being a complex fluid mechanical phenomenon, the coiling of viscous fluids can be studied using the simple approach of deriving scaling laws. Different mechanisms balance viscous forces in a liquid rope depending on its fall height, resulting in three distinct coiling regimes: viscous, gravitational and inertial.

The gravitational stretching of the jet and the dependency of the coiling frequency on the fall height were studied experimentally for the gravitational and inertial regimes. The trend $a_1 \propto H^{-1}$ was observed for the parameter range $3 \text{ cm} < H < 8.5 \text{ cm}$. The scaling laws obtained for the coiling frequency $\alpha_G = 1.81 \pm 0.33$ and $\alpha_I = 3.09 \pm 0.24$ are in good agreement with the ones predicted by theory for the gravitational and inertial regimes, respectively. A full numerical solution of the problem is left as further work, allowing a more profound quantitative analysis of the coiling frequencies obtained experimentally.

ACKNOWLEDGEMENTS

I thank Professor Filipe Joaquim for the fruitful discussions and guidance throughout this project. I also thank my father, José Manuel Cruz, for helping me build the experimental apparatus and take the measurements in time record intervals. Finally, I thank my colleagues and friends Victor Hariton, André Lopes and José Lopes for their constructive reviews of this article.

-
- [1] R. W. Griffiths and J. S. Turner. Folding of viscous plumes impinging on a density or viscosity interface. *Geophysical Journal*, 95(2):397–419, 1988.
- [2] M. F. Tome and Sean McKee. Numerical simulation of viscous flow: Buckling of planar jets. *International Journal for Numerical Methods in Fluids*, 29(6):705–718, 1999.
- [3] G. Barnes and R. Woodcock. Liquid rope-coil effect. *American Journal of Physics*, 26(4), 1958.
- [4] G.I. Taylor. Instability of jets, threads, and sheets of viscous fluid. pages 382–388, 1969.
- [5] N. M. Ribe. Coiling of viscous jets. *Royal Society of London Proceedings Series A*, 460:3223–3239, November 2004.
- [6] Minitrem ®. <http://www.minitrem.com.pt>.
- [7] D. Brown and W. Christian. Simulating what you see. In *MPTL 16*, Ljubljana, Slovenia, Sept 15-17 2011.